Numerical calculations of the ionization of one-dimensional hydrogen atoms using hydrogenic and Sturmian basis functions

S. M. Susskind* and R. V. Jensen
Mason Laboratory, Yale University, New Haven, Connecticut 06520
(Received 5 November 1986; revised manuscript received 22 January 1988)

Exact integral expressions and simple analytical estimates for the bound-bound, bound-continuum, and continuum-continuum dipole matrix elements are derived by use of the momentum-space eigenfunctions for a one-dimensional model of a hydrogen atom. These results provide the essential ingredients for the numerical study of the quantum mechanisms responsible for the chaotic ionization of highly excited hydrogen atoms in intense microwave fields. A specific numerical algorithm for solving the Schrödinger equation for a one-dimensional hydrogen atom in an oscillating electric field is described which uses these results for the dipole matrix elements along with a discrete representation of the continuum. In addition, the momentum-space representation of the Sturmian basis functions has been used to derive exact integral expressions and convenient analytical estimates for the projections of the Sturmian basis functions onto the hydrogenic bound and continuum states. These results are used to provide a direct comparison of numerical calculations for the ionization of one-dimensional hydrogen atoms using the hydrogenic and Sturmian bases.

I. INTRODUCTION

Recently, there has been considerable interest in the quantum behavior of dynamical systems, such as coupled nonlinear oscillators or periodically driven nonlinear oscillators, which can exhibit chaotic behavior in the classical limit.[1] This research has been greatly stimulated by the possibility of observing the manifestations of "quantum chaos" in experiments with simple systems such as Rydberg atoms in strong static and oscillating fields.[1] In particular, the experiments on the ionization of highly excited hydrogen atoms by intense microwave fields pioneered by Bayfield and Koch[2] have provided an ideal opportunity to study the behavior of a quantum system which is classically chaotic.

In the classical limit the electron executes Keplerian motion about the nucleus which is perturbed by the oscillating electric field. If the microwave perturbation exceeds a critical threshold, then the behavior of this classical nonlinear oscillator exhibits a dramatic transition from regular, bounded orbits to chaotic, unbounded electron trajectories which ionize.[3-5] The experiments also show a sharp threshold for the microwave field required for significant ionization, which is in remarkable agreement with the classical numerical calculations for the onset of chaotic ionization for a wide range of initial quantum states, $n=32-90$.[6]

These experimental results indicate that the effects of classical chaos can persist in simple quantum systems. The challenge now remains to determine the quantum mechanism which accounts for the sharp ionization threshold as a function of microwave intensity and to understand how the classical ionization is modified by purely quantum-mechanical interference effects and resonant multiphoton processes. The theoretical difficulty lies in the facts that 100 or more 9.92-GHz photons are required for ionization in the experiments and that the perturbing electric fields are too large, approximately 10% of the Coulomb binding field, for conventional time-dependent perturbation theory to be useful. Consequently, the development of the theory must depend heavily on numerical studies of the quantum dynamics.

Fortunately, the threshold for chaotic ionization is well described by a one-dimensional classical model of the experiment[4-6] defined in atomic units (a.u.) by the Hamiltonian $H(x,p,t)=H_0(x,p)+V(x,t)$ with

$$H_0=\frac{p^2}{2}+\begin{cases}\infty, & x\le 0\\ -1/x, & x>0\end{cases}$$
$$V=xF(t)\cos(\Omega t)\ , \tag{1}$$

corresponding to a one-dimensional hydrogen atom in an oscillating electric field with frequency Ω with a time-varying amplitude $F(t)$ which models the slow turn-on and turn-off of the microwave perturbation. As a consequence, we can hope that a quantum theory based on the corresponding one-dimensional Schrödinger equation,

$$i\frac{\partial\phi}{\partial t}=-\frac{1}{2}\frac{\partial^2\phi}{\partial x^2}-\frac{1}{x}\phi+xF(t)\cos(\Omega t)\phi,\quad x\ge 0 \tag{2}$$

will capture much of the essential physics of the chaotic ionization observed in the experiments. Faster computers and more efficient numerical algorithms are required for a practical numerical solution of the three-dimensional Schrödinger equation which provides a full description of the atoms studied in the recent experiments by van Leeuwen and Koch.[6] The one-dimensional theory also has important applications to other physical systems which are well described by the one-dimensional Hamiltonian, Eq. (1), such as surface-state electrons[4] or

electrically polarized states of highly excited hydrogen atoms.[7]

The success of the one-dimensional classical theory has motivated many people[8–11] to investigate detailed numerical solutions of the one-dimensional Schrödinger equation, Eq. (2). However, even the one-dimensional model calculations have proven to be surprisingly difficult. The principal complication lies in developing approximate numerical algorithms for the calculation of the coupling to the continuum states which is essential for understanding the ionization mechanism.

In Sec. II we begin by describing a numerical procedure for expanding the solutions of the Schrödinger equation in terms of the bound and continuum eigenstates of the unperturbed hydrogen atom. This numerical algorithm requires accurate and convenient expressions for the dipole matrix elements for the bound-bound, bound-continuum, and continuum-continuum transitions. One of the primary purposes of this paper is to present a simple method for deriving exact formulas and useful analytical estimates for the required matrix elements using the momentum-space representation of the hydrogenic eigenfunctions. In Sec. III the exact integral expressions and analytical approximations for the matrix elements are derived. In Sec. IV we describe a method for discretizing the continuum which reduces Eq. (2) to a finite system of ordinary differential equations with coupling coefficients determined by the results of Sec. III. In addition, Sec. IV provides an explicit description of our numerical procedure for solving this system of coupled equations, using both the $x\cdot E$ and $p\cdot A$ representation of the interaction with the oscillating electric field.

The coupling of the bound states to the continuum for a one-dimensional hydrogen atom has also been studied by Blümel and Smilanksy[10] using a projection operator method which neglects the continuum-continuum coupling and by Casati *et al.*[8] using Sturmian basis functions. Although these approaches may have some numerical advantages, our method describes the quantum dynamics in terms of the familiar concepts of bound and continuum states which facilitates the physical interpretation of the results. In addition, by varying the number and density of continuum states we can easily assess and control the accuracy of our calculation.

In an effort to determine the advantages and disadvantages of our numerical procedure as well as the accuracy of our results, we have also performed numerical calculations of the ionization of one-dimensional hydrogen atoms using the Sturmian basis functions which also provide a discrete representation of the continuum. We use the momentum-space representation of the Sturmian functions in Sec. V to determine the coupling coefficients among the Sturmian states and, more importantly, to derive exact integral expressions and simple analytical approximations for the projections of the Sturmian states onto the bound and continuum states of the unperturbed hydrogen atom. These latter results, which appear to be new, are essential for assessing the amounts of ionization and for comparing the two types of calculations.

In Sec. VI we provide an illustration of these numerical methods by presenting a comparison of the results of our numerical calculations with a discretized continuum in both the $x\cdot E$ and $p\cdot A$ gauges with the results of a corresponding Sturmian calculation for a model problem consisting of a one-dimensional hydrogen atom initially in the $n_0=20$ state perturbed by strong oscillating electric fields with a scaled frequency of $n_0^3\Omega=1.0$ (a.u.).

Finally, in Sec. VII we summarize our results and we briefly discuss potential applications of our numerical studies of one-dimensional hydrogen atoms to the microwave ionization of highly excited hydrogen atoms and to other problems involving the interaction on intense radiation with matter, such as the process of above-threshold ionization.

II. HYDROGENIC BASIS FUNCTIONS

The most direct approach to the solution of Eq. (2) is to expand $\phi(x,t)$ in terms of the bound and continuum eigenfunctions of the unperturbed Hamiltonian H_0,

$$\phi(x,t)=\sum_{n=1}^{\infty} a_n(t)\phi_n(x)+\int_0^{\infty} dk\, a_k(t)\phi_k(x)\ . \tag{3}$$

Then in the interaction representation with $b_n(t)=a_n(t)e^{-i\epsilon_n t}$ and $b_k(t)=a_k(t)e^{-i\epsilon_k t}$, where $\epsilon_{n,k}$ are the corresponding eigenvalues of H_0, the Schrödinger equation can be formally expressed as an infinite set of linear differential equations

$$i\frac{db_n}{dt}=\sum_m W_{nm}b_m+\int_0^{\infty} dk\, W_{nk}b_k dk\ , \tag{4}$$

$$i\frac{db_k}{dt}=\sum_m W_{km}b_m+\int_0^{\infty} dk' W_{kk'}b_{k'}dk'\ , \tag{5}$$

where the coupling coefficients

$$W_{ab}=e^{i\omega_{ab}t}F(t)\cos(\Omega t)x_{ab}$$

depend on the values of the Bohr frequencies $\omega_{ab}=\epsilon_a-\epsilon_b$ and the dipole matrix elements $x_{ab}=\langle a\mid x\mid b\rangle$ for the bound and continuum wave functions with $a,b=n,k$.

In order to solve Eqs. (4) and (5) we must first compute the bound-bound, bound-continuum, and continuum-continuum matrix elements of x with respect to the eigenfunctions of H_0. Other numerical studies of this problem[8–10] have generally relied on the representation of the matrix elements of x in terms of hypergeometric functions derived by Gordon in 1929 for three-dimensional wave functions in spherical and parabolic coordinates.[12,13] In particular, for large n the matrix elements for the extremal parabolic states with $n_2=n-1$, $n_1=0$, and $m=0$ provide excellent approximations for the one-dimensional matrix elements. However, the computation of the matrix elements for bound states with large principal quantum numbers and for continuum states can be very involved, requiring explicit evaluation of the very large order polynomials or infinite series which represent the corresponding hypergeometric functions. Approximate formulas for the bound-bound and bound-free matrix elements for large n have also been derived by Gore-

lavskii *et al.*[14] using WKB wave functions. They succeeded in giving a good approximation for bound-bound matrix elements. However, they derived the bound-continuous matrix elements by analytic continuation of the bound-bound result which introduces an ambiguity since the normalization of the continuum wave functions is not specified by the prescription. Finally, no one appears to have previously derived useful expressions for the continuum-continuum matrix elements for the Coulomb potential.

In contrast we have derived exact integral representations for the bound-bound, bound-continuum, and continuum-continuum matrix elements of the one-dimensional hydrogen atom which can either be evaluated by direct numerical integration or approximated by analytical means. Starting from first principles we transform the one-dimensional eigenvalue equation for H_0 to a first-order, ordinary differential equation for the momentum-space eigenfunctions which is easily solved for both negative and positive eigenvalues. These exact analytical expressions for the bound and continuum wave functions are then used in Sec. III to evaluate the diagonal and off-diagonal matrix elements of x in terms of integrals over the momentum p. In each case useful analytical estimates for the matrix elements are derived from the exact integral representations. The estimates of the bound-bound and bound-continuum matrix elements for large n are in agreement with the results derived previously by Goreslavskii *et al.*;[14] however, our first-principles calculation clarifies both the nature of the approximations involved in deriving these formulas as well as the range of validity. In addition, we provide the first useful expressions for the continuum-continuum matrix elements which can play an important role in the calculation of the ionization of one-dimensional hydrogen atoms in external fields.

A. Schrödinger equation in momentum space

The Schrödinger equation in x space for the eigenfunctions of the unperturbed Hamiltonian H_0 is

$$-\frac{1}{2}\frac{d^2\phi_\epsilon}{dx^2}-\frac{1}{x}\phi_\epsilon=\epsilon\phi_\epsilon, \quad x\geq 0 \tag{6}$$

where $\phi_\epsilon=0$ for $x\leq 0$. Introducing the p-space wave function by

$$\psi_\epsilon(p)=(2\pi)^{-1/2}\int_0^\infty \phi_\epsilon(x)e^{-ipx}dx \ , \tag{7}$$

Eq. (6) transforms to[15]

$$(\epsilon-p^2/2)\frac{d\psi_\epsilon}{dp}=(p+i)\psi_\epsilon \ , \tag{8}$$

which is an equation of first order for $\psi_\epsilon(p)$. From Eq. (7) it follows that the integration path of the inverse Fourier transform that recovers $\phi_\epsilon(x)$ should be, in principle, in the lower half of the p plane.

B. Discrete spectrum (Ref. 16)

For negative energies, $\epsilon=-|\epsilon|$, the direct integration of Eq. (8) gives

$$\psi_\epsilon(p)=\frac{B}{(|\epsilon|+p^2/2)}\exp[i\sqrt{2/|\epsilon|}\cot^{-1}(p/\sqrt{2|\epsilon|})] \ , \tag{9}$$

where B is a constant to be specified by normalization. Since $\psi_\epsilon(p)$ must be single valued and the $\cot^{-1}$ function has a period of π, we must have

$$\left[\frac{2}{|\epsilon|}\right]^{1/2}\pi=2n\pi, \quad n \text{ integer} \tag{10}$$

which requires that the negative eigenvalues be discrete with values $\epsilon=-1/2n^2$. Normalizing the associated eigenfunction, we finally obtain

$$\psi_n(p)=\left[\frac{2n}{\pi}\right]^{1/2}\frac{1}{(1+n^2p^2)}\exp[2in\cot^{-1}(np)]$$

$$=\left[\frac{2n}{\pi}\right]^{1/2}\frac{(np+i)^{n-1}}{(np-i)^{n+1}} \ . \tag{11}$$

One can check that the Fourier transform of Eq. (11) gives the well-known result for $\phi_n(x)$ in terms of Laguerre polynomials.[17]

C. Continuous spectrum

For positive energies, $\epsilon=k^2/2$, Eq. (8) gives

$$\psi_k(p)=C\frac{1}{(p^2-k^2)}\left[\frac{p+k}{p-k}\right]^{i/k} \ , \tag{12}$$

where k can assume any positive value. The integration constant C is determined by normalizing ψ_k to a δ function in k,[13]

$$\int_{-\infty}^{\infty}\psi_{k'}^*(p)\psi_k(p)dp=\delta(k'-k) \ . \tag{13}$$

Finally, after some calculations described in Appendix A, we obtain

$$\psi_k(p)=\left[\frac{2k}{\pi}\right]^{1/2}\frac{1}{(1-e^{-2\pi/k})^{1/2}}\frac{1}{(p^2-k^2)}\left[\frac{p+k}{p-k}\right]^{i/k} \ . \tag{14}$$

If, instead of Eq. (13), an energy normalization for the continuum eigenfunctions is preferred [i.e., to a $\delta(\epsilon'-\epsilon)$], then the result (14) is simply modified to $\psi_\epsilon=\psi_k/\sqrt{k}$. Again, it can be checked that by Fourier transforming Eq. (14) one obtains the well-known result for $\phi_k(x)$ in terms of hypergeometric functions.

III. MATRIX ELEMENTS OF x AND p

To compute the off-diagonal matrix elements of the x operator using the momentum-space wave functions, Eqs. (11) and (14), we use the well-known relation to the matrix elements of p,

$$(\epsilon-\epsilon')\langle\epsilon' \mid x \mid \epsilon\rangle = i\langle\epsilon' \mid p \mid \epsilon\rangle \ , \tag{15}$$

which is obtained by computing the matrix elements of $[x,H]=ip$ between the eigenfunctions of H_0 with discrete or continuous values of ϵ and ϵ'.

A. Bound-bound (B-B)

Substituting the bound-state wave functions in momentum space given by Eq. (11) into Eq. (15), we obtain an integral representation for the B-B matrix element,

$$\langle n' \mid x \mid n\rangle = -\frac{8}{\pi}\frac{(nn')^{5/2}}{(n'^2-n^2)}\int_0^\infty \frac{p\sin[2n'\cot^{-1}(n'p)-2n\cot^{-1}(np)]}{(1+n'^2p^2)(1+n^2p^2)}dp \ , \tag{16}$$

which is easily evaluated numerically. Moreover, for large values of n,n' with $n'>n$ (say), we obtain a very good approximation to Eq. (16) by splitting the integral as

$$\int_0^\infty = \int_0^{1/n'} + \int_{1/n'}^\infty \ . \tag{17}$$

Since the integrand is zero at $p=0$, the first integral can be approximated by zero for large n'. For the second term we neglect 1 compared with np and $n'p$ in the denominator of the integrand and expand the argument of the sine to first nonvanishing order (third order) in $1/np$, $1/n'p$. After a change of variables we get

$$\langle n' \mid x \mid n\rangle \simeq -\frac{3^{-1/3}2^{7/3}}{\pi}\frac{(nn')^{11/6}}{(n'^2-n^2)^{5/3}} \times g\left[\frac{2}{3}\frac{n'}{n^2}(n'^2-n^2)\right] , \tag{18}$$

where

$$g(\eta)=\int_0^\eta t^{-1/3}\sin t\,dt \ . \tag{19}$$

For $n'-n \gg 1$ we can replace the function g by its limiting value $g(\infty)=\sqrt{3}/2\Gamma(2/3)$ (Ref. 17), and Eq. (18) can be finally reduced to

$$\langle n' \mid x \mid n\rangle \simeq -\frac{2^{4/3}3^{1/6}}{\pi}\Gamma(2/3)\frac{(nn')^{11/6}}{(n'^2-n^2)^{5/3}} \tag{20}$$

for large n,n' ($n' \gg n$). However, in practice we find that Eq. (20) provides a good approximation to Eq. (16) even for $n'-n\sim 1$. For example, Fig. 1 shows a comparison of the exact values of the matrix elements for $n,n'\sim 40$, calculated by a direct numerical integration of Eq. (16), with the approximate values given by Eq. (20).

Equation (20) also agrees with the result obtained in Ref. (14) using WKB wave functions. Moreover, Eq. (20) coincides, as it should because of the correspondence principle,[13] with the $(n'-n)$ Fourier component of the position coordinate x in the classical problem.[4,5]

The bound state eigenfunctions of the one-dimensional hydrogen atom also have a permanent dipole moment given by the diagonal matrix elements of x which can be evaluated directly using $\psi_n(p)$ by replacing x by $i(d/dp)$ to obtain the well-known result

$$\langle n \mid x \mid n\rangle = \tfrac{3}{2}n^2 \ . \tag{21}$$

B. Bound-continuum (B-C)

To obtain the B-C matrix elements, we substitute Eqs. (11) and (14) into (15) and integrate along a path that goes around the singularities $p=\pm k$ of ψ_k in the lower half of the complex p plane. We choose as the branch cut the segment between $-k$ and k and perform the integral below the real axis. We find that the contributions from the logarithmic branch points are zero. The only contribution to the integral is

$$\langle n \mid x \mid k\rangle = -\frac{8}{\pi}\frac{n^{5/2}}{(1+n^2k^2)}\frac{k^{1/2}}{(1-e^{-2\pi/k})^{1/2}}\int_0^\infty \frac{p\sin\left[\frac{1}{k}\ln\left|\frac{p+k}{p-k}\right|-2n\cot^{-1}(np)\right]}{(1+n^2p^2)(p^2-k^2)}\exp\left[-\frac{1}{k}\arg\left[\frac{p+k}{p-k}\right]\right]dp \ , \tag{22}$$

where it should be regarded as a principal value integral in passing through k.

Note that in passing right below the real axis, the

$$\exp\left[-\frac{1}{k}\arg\left[\frac{p+k}{p-k}\right]\right]$$

factor in the integrand changes the integral to

$$\int_0^\infty = e^{-\pi/k}\int_0^k + \int_k^\infty \ , \tag{23}$$

while the rest of the integrand stays the same as in Eq. (22). From this last expression, we can see that the major contribution for $k\to 0$, correct to exponentially small terms, is going to be given by the second integral. We can also see that this is consistent with our choice of contour in the inverse of Eq. (7). If we would have chosen the upper p plane, we would have had an $e^{\pi/k}$ factor which diverges for $k\to 0$ and hence inconsistent with the problem at hand.

The exact representation, Eq. (22), for the B-C matrix

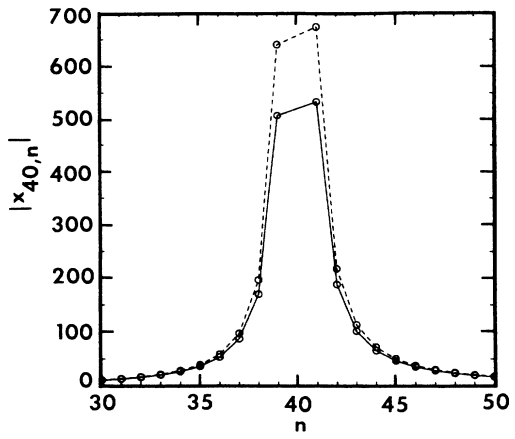

FIG. 1. Approximate formula, Eq. (20), for the absolute values of the bound-bound matrix elements $x_{nn'}$, with $n,n' \sim 40$ (dashed line), is compared with the numerical integration of the exact expression, Eq. (20) (solid line).

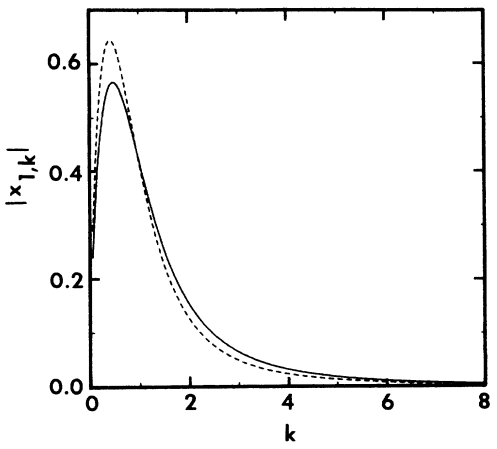

FIG. 2. Approximate formula, Eq. (24), for the bound-continuum matrix elements x_{nk}, for $n=1$ and for small k (dashed line), is compared with the exact analytical values for $\langle 1 \mid x \mid k \rangle$ (solid line) obtained from Eq. (25).

elements can also be evaluated numerically, by separating the integral between 0 and k and between k and ∞ and changing the variable to $t=(p+k)/(p-k)$, which sends the singularities to $\pm\infty$. Moreover, a very good analytical approximation of Eq. (22) can be obtained for large n by a procedure similar to the B-B case.

First, we divide the integral between 0 and k (or $1/n$, whichever is bigger) and between k (or $1/n$) and ∞. For small k and large n, we neglect the first term as before [see also Eq. (23)], and expand the integrand in the second term for small k/p and $1/np$, to get

$$\langle n \mid x \mid k \rangle \simeq -\frac{2^{4/3}3^{1/6}}{\pi}\Gamma(2/3)\frac{n^{11/6}k^{1/2}}{(1+n^2k^2)^{5/3}} . \quad (24)$$

This approximation is in good agreement with the exact matrix elements even for $n \sim 1$ and for large values of k. For example, Fig. 2 shows a comparison of Eq. (24) with the exact B-C matrix element for $n=1$,

$$\langle 1 \mid x \mid k \rangle = -\frac{8k^{1/2}}{(1-e^{-2\pi/k})^{1/2}}\frac{e^{-(2/k)\tan^{-1}k}}{(1+k^2)^2} , \quad (25)$$

which can be determined from the x-space wave functions and the properties of hypergeometric functions given in Ref. 13.

C. Continuum-continuum (C-C)

From Eqs. (14) and (15) and after similar considerations as in the previous case regarding the singularities at k and k' we get

$$\langle k' \mid x \mid k \rangle = -\frac{8}{\pi}\frac{(k'k)^{1/2}}{(k'^2-k^2)}\frac{1}{(1-e^{-2\pi/k'})^{1/2}}\frac{1}{(1-e^{-2\pi/k})^{1/2}}\int_0^\infty \frac{p\sin\left[\frac{1}{k'}\ln\left|\frac{p+k'}{p-k'}\right|-\frac{1}{k}\ln\left|\frac{p+k}{p-k}\right|\right]}{(p^2-k'^2)(p^2-k^2)}$$
$$\times\exp\left[-\frac{1}{k'}\arg\left[\frac{p+k'}{p-k'}\right]\right]$$
$$\times\exp\left[-\frac{1}{k}\arg\left[\frac{p+k}{p-k}\right]\right]dp . \quad (26)$$

Again, for small k and $k'>k$, we divide the integral into two terms, neglect the first term, and expand the integrand in the second for small k/p and k'/p, to obtain the approximate expression

$$\langle k' \mid x \mid k \rangle \simeq -\frac{3^{-1/3}2^{7/3}}{\pi}\frac{(kk')^{1/2}}{(k'^2-k^2)^{5/3}}g\left[\frac{2}{3k'^3}(k'^2-k^2)\right] , \quad (27)$$

where g is given by Eq. (19). Finally, for $(k'-k)/k'^2 \gg 1$ we can use the limiting value of $g(\infty)$ to arrive at

$$\langle k' \mid x \mid k \rangle \simeq -\frac{2^{4/3}3^{1/6}}{\pi}\Gamma(2/3)\frac{(kk')^{1/2}}{(k'^2-k^2)^{5/3}} . \quad (28)$$

Figure 3 displays a comparison of Eq. (28) with the results of a direct numerical integration of Eq. (26), which shows that Eq. (28) provides a good approximation for the C-C matrix elements even for $k'-k \sim k'^2$.

For $k' \to k$, Eq. (28) says that the singularity of $x_{k'k}$ goes as approximately $(k'-k)^{-5/3}$. However, a clever argument due to Gontier[18] shows that the exact exponent of the singularity should be 2 instead of $\frac{5}{3}$. The argument goes as follows: from $[p, H_0] = -i/x^2$ we have for $\epsilon' \neq \epsilon$

$$(\epsilon-\epsilon')\langle \epsilon' \mid p \mid \epsilon \rangle = -i\left\langle \epsilon' \left| \frac{1}{x^2} \right| \epsilon \right\rangle . \quad (29)$$

Now, since $\langle \epsilon' \mid 1/x^2 \mid \epsilon \rangle$ must be positive and finite, then $\langle \epsilon' \mid p \mid \epsilon \rangle$ diverges as $(\epsilon'-\epsilon)^{-1}$, and by Eq. (15) $\langle \epsilon' \mid x \mid \epsilon \rangle$ goes as $(\epsilon'-\epsilon)^{-2}$ for $\epsilon' \to \epsilon$, $\epsilon' \neq \epsilon$. This difference in the exponent between $\frac{5}{3}$ and 2 explains why the exact expression for $x_{k'k}$ lies above the approximate expression for $k' \to k$ in Fig. 3.

The evaluation of the contribution of the diagonal C-C matrix elements $\langle k \mid x \mid k \rangle$ is more involved and this quantity is divergent. In fact, a close examination of Eq. (15) shows that the general solution for $\langle k' \mid x \mid k \rangle$ as $k' \to k$ should also include a δ-function term. If we think of discretizing the continuum states by putting the atom in a large box, the coefficient of the δ-function term will be proportional to L, the size of the box (see Appendix B),

$$\langle k' \mid x \mid k \rangle = -\frac{2i}{(k'^2-k^2)}\langle k' \mid p \mid k \rangle + L\delta(k'-k) . \quad (30)$$

The first term in this expression is given by Eq. (26). This term, as seen above, also diverges for $k' \to k$. However, what is really needed for any calculation (see Sec. IV) is the integral

$$\lim_{\Delta \to 0} \int_{k-\Delta/2}^{k+\Delta/2} dk' \langle k' \mid x \mid k \rangle , \quad (31)$$

which represents physically the contribution of the diagonal matrix element x_{kk} plus the contributions of nearby continuum states. Upon calculating this integral, using the two term expression given by Eq. (30), both divergences cancel out. This is shown in Appendix B. The fact that both divergent and opposite terms have to give a finite result upon integration in an interval Δ of k' is clear from Eq. (5). If it were not so, the right-hand-side term would diverge unless the b_k's are all zero.

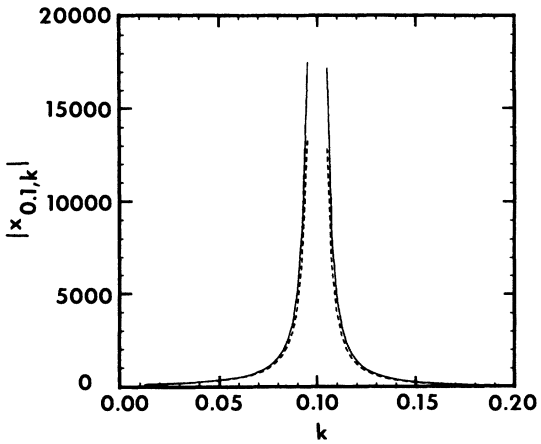

FIG. 3. Approximate formula Eq. (28), for the continuum-continuum matrix elements $x_{kk'}$ (dashed line), is compared with the numerical integration of the exact expression, Eq. (26) (solid line), for $k, k' \sim 0.1$.

IV. NUMERICAL SOLUTION USING HYDROGENIC BASIS FUNCTIONS

A. Discretization of the continuum

Now that we have obtained useful expressions for the matrix elements, we would like to put Eqs. (4) and (5) in a form suitable for numerical calculations by introducing a discrete representation of the continuum.[19] Since the positive-energy eigenfunctions are labeled by the continuous index k, we divide the k axis between $[0, k_{\max}]$ into N_c segments, each centered at k_j, $j = 1, N_c$, with width Δ_j. Then the integral over the continuum states in Eq. (4) can be approximated by

$$\int_0^\infty dk\ W_{nk} b_k \simeq \sum_{j=0}^{N_c} \int_{k_j-\Delta_j/2}^{k_j+\Delta_j/2} dk\ W_{nk} b_k , \quad (32)$$

and as long as $W_{nk} b_k$ varies little on the scale of Δ_j we can replace each term in the sum by $W_{nk_j} b_{k_j} \Delta_j$.

Similarly, in Eq. (5) we approximate

$$\int_0^\infty dk' W_{kk'} b_{k'} \simeq \sum_{\substack{j=0 \\ k \neq k_j}}^{N_c} \int_{k_j-\Delta_j/2}^{k_j+\Delta_j/2} dk' W_{kk'} b_{k'} + \int_{k-\Delta/2}^{k+\Delta/2} dk' W_{kk'} b_{k'} , \quad (33)$$

where each term of the sum can again be replaced by $W_{kk_j} b_{k_j} \Delta_j$ as before. However, because of the divergence of the C-C matrix elements, the last term in Eq. (33) must be treated with care. (See Appendix B.)

With this scheme, we can put the bound states and the discretized continuum on the same footing by truncating the bound states to a finite number N_b and expressing our problem in terms of a large set of linear, ordinary differential equations. If all of the Δ_j are chosen to be equal, then this prescription is essentially equivalent to putting the one-dimensional hydrogen atom in a large box of length proportional to $1/\Delta_j$. More generally we have the flexibility of varying Δ_j as well as $k_{\max}$ to optimize the coverage of the range of k where most of the coupling from the bound states to the continuum occurs. In

addition, we find in practice that resonant multiphoton processes from the bound states give rise to prominent peaks in the distribution over the continuum states which grow in time. Consequently, the assumptions used to discretize the continuum fail after a period of time which can be increased by decreasing Δ_j and increasing the number of states. However, by carefully monitoring the evolution of the probability distribution over continuum states we can easily detect and remedy any failures in the approximations.

B. Calculations in the $x \cdot E$ gauge

Unfortunately, the singular off-diagonal C-C matrix elements and the divergent diagonal C-C matrix elements in Eq. (33) create serious numerical problems for the solution of the full set of equations using the $x \cdot E$ representation of the coupling to the electromagnetic field. Although we show in Appendix B that the divergences in Eq. (33) cancel in the limit $\Delta_j \to 0$, it is difficult to maintain this cancellation in a numerical calculation with finite Δ_j. As a consequence the numerical calculations in the $x \cdot E$ gauge required that the C-C coupling be neglected altogether. In many cases the neglect of the C-C interaction can be justified and the neglect of these troublesome terms is not a bad approximation.[20] However, in other problems, such as the interaction of intense laser radiation with ground-state atoms, the C-C coupling plays a very important role.[21,22] Nevertheless, since the C-C coupling can be turned back on using the $p \cdot A$ gauge or by using the Sturmian basis functions as described in subsequent sections, the validity of this approximation can be checked for individual cases.

Therefore, by neglecting the C-C coupling in the $x \cdot E$ representation of the perturbation, we reduce the Schrödinger equation to a large linear system of coupled, ordinary differential equations of the form

$$i\frac{dy_s}{dt} = F(t)\cos(\Omega t)\sum_{r=1}^{N_b+N_c} z_{sr} e^{i\omega_{sr}t} y_r \ , \tag{34}$$

where $y_r = b_r$ for bound states, $y_r = \Delta_r^{1/2} b_{k_r}$ for continuum states, and the coupling coefficients are given by

$$z_{sr} = \begin{cases} x_{sr} & \text{for } s \text{ and } r \text{ bound} \\ \Delta_s^{1/2} x_{k_s r} & \text{for } s \text{ continuum and } r \text{ bound} \\ 0 & \text{for } s \text{ and } r \text{ continuum} \ . \end{cases} \tag{35}$$

Finally, we can improve the numerical efficiency of solving Eq. (34) by eliminating the diagonal couplings with the transformation

$$y_r = c_r \exp[-iz_{rr}\int F(t)\cos(\Omega t)dt] \ . \tag{36}$$

Then Eq. (34) can be rewritten as

$$i\frac{dc_s}{dt} = F(t)\cos(\Omega t)\sum_{r\neq s}^{N_b+N_c} z_{sr} e^{i\phi_{sr}(t)} c_r \ , \tag{37}$$

where

$$\phi_{sr}(t) = \omega_{sr}t + (z_{ss} - z_{rr})\int F(t)\cos(\Omega t)dt \ .$$

This is the most convenient form from the point of view of numerical calculations since the diagonal matrix elements are the largest coefficients and they make the right-hand side of Eq. (34) very large, slowing down the integration considerably.

For the interpretation of $P_r = |y_r|^2$ as the probability of being in the state r, discrete or continuum, to be valid, we have to verify that the total probability $P_{\rm tot} = \sum_{r=1}^{N_b+N_c} y_r^* y_r$ is a constant in time for any number of bound, N_b, and continuum, N_c, states used in the calculations. This can be easily verified from the hermiticity property of Eq. (34). Taking the derivative of $P_{\rm tot}$,

$$\frac{dP_{\rm tot}}{dt} = \sum_{r=1}^{N_t} \frac{dy_r^*}{dt} y_r + \sum_{r=1}^{N_t} y_r^* \frac{dy_r}{dt} \ , \tag{38}$$

replacing the derivatives by Eq. (34) and its complex conjugate, and using the hermiticity of $z_{sr}e^{i\omega_{sr}t}$, we obtain $dP_{\rm tot}/dt = 0$ for any $N_t = N_b + N_c$. We then choose $P_{\rm tot}(0) = 1$ initially; this value is kept to numerical accuracy throughout the calculation.

Note also that the y_r's, which represent the probability amplitudes of the discretized continuum, are invariant under a change of the continuum label. We were using in all of our discussions above the continuum label k such that the energy of the continuum states is $\epsilon = k^2/2$. If we want to use the ϵ label, then $y_{\epsilon_r} = \Delta_{\epsilon_r}^{1/2} b_{\epsilon_r}$. But $\Delta_{\epsilon_r} = k_r \Delta_{k_r}$ and $b_{\epsilon_r}/\sqrt{k_r}$, as seen before, so $y_{\epsilon_r} = y_{k_r} = y_r$.

C. Calculations in the $p \cdot A$ gauge

If it is necessary to include the contributions of the C-C interactions, then the numerical calculations are much easier in the $p \cdot A$ representation of the interaction with the oscillating electric field.

In the $p \cdot A$ gauge the Hamiltonian for a one-dimensional hydrogen atom in an oscillating electric field is

$$H = \tfrac{1}{2}[p + A(t)]^2 - \frac{1}{x} = \tfrac{1}{2}p^2 + pA + \tfrac{1}{2}A^2 - \frac{1}{x} \ , \tag{39}$$

where $A(t) = -\int F(t)\cos(\Omega t)dt$. Since the $\frac{1}{2}A^2$ term only contributes to a global phase factor, we will neglect it in the integration of the corresponding equations of motion. In this case the coupling of the atom to the oscillating electric field depends on the matrix elements of p.

If we expand the wave function as

$$|\psi\rangle = \sum_r b_r(t) e^{-i\epsilon_r t} |\psi_r\rangle \ ,$$

where r denotes a discrete or continuum state, we obtain after substituting this expansion in the Schrödinger equation corresponding to Eq. (39)

$$i\frac{db_s}{dt} = A(t)\sum_{r\neq s} p_{sr} e^{i\omega_{sr}t} b_r \ , \tag{40}$$

where the relation given by Eq. (15) says that

$p_{sr}=i\omega_{sr}x_{sr}$.

Comparing Eq. (40) with Eq. (34), we see that each term of the right-hand side of Eq. (40) is approximately ω_{sr}/Ω times the corresponding term in Eq. (34). When r and s are continuum states, this is an advantage because the divergent diagonal matrix elements are eliminated altogether and the singularity of the off-diagonal matrix elements for nearby continuum states is greatly reduced. However, in situations in which the B-B and B-C transitions play the most important roles and where a large number of photons are involved, as in the microwave ionization experiments, the B-B and B-C coupling in Eq. (40) becomes very large, as $\omega_{sr}/\Omega \gg 1$, making the numerical integration of this equation very slow.

V. NUMERICAL SOLUTION USING THE STURMIAN BASIS FUNCTIONS

In this section we consider the numerical solution of the Schrödinger equation for a one-dimensional hydrogen atom in an oscillatory electric field using Sturmian basis functions. This provides us with an alternative approach to the problem which can be compared both for accuracy and numerical efficiency with the algorithms using a boxed-continuum described in Sec. IV.

As is well known, the Schrödinger equation can be expressed in any complete set of basis functions. For problems involving the interaction of an atom with a strong static electric or magnetic field,[23] the so-called Sturmian basis functions are often preferred over the eigenfunctions of the unperturbed atom. The Sturmian basis is a particular basis set which has the advantage of being complete and discrete. These properties makes them convenient to use in problems in which continuum effects are important, without having to deal with the inconveniences caused by the use of continuum wave functions, such as discretizing the continuum for numerical calculations or dealing with singular matrix elements. Another advantage is that the matrix elements in the equations of evolution are very easy to evaluate and are given by simple algebraic expressions, with no hypergeometric functions. However, the price paid for these advantages is primarily the loss of the physical intuition contained in the hydrogen basis, to which one is familiar and in terms of which all experimental situations are described. As a consequence the results of the Sturmian calculations must be projected back onto the basis of bound and continuum hydrogenic states to provide a detailed interpretation of the results. In general this projection resurrects the necessity of evaluating complex expressions involving hypergeometric functions. In addition, because there is no one-to-one correspondence between the hydrogenic and Sturmian basis functions it is difficult to control the accuracy of the Sturmian representation of the highly excited bound states and low energy continuum states. If these states play an important role, then numerical calculations require at least twice as many Sturmian functions to achieve the same resolution as carefully chosen bound and discretized continuum states of the hydrogenic basis.

Nevertheless, the advantages of the Sturmian basis functions have led Casati *et al.*[8] to use them for numerical studies of the microwave ionization of highly excited hydrogen atoms. Using up to 480 Sturmian basis functions they have solved the Schrödinger equation for a one-dimensional hydrogen atom in an oscillating electric field. Then by recursively evaluating the hypergeometric functions in the formal expressions for the projection onto the bound states of the hydrogenic basis, they have performed a number of very interesting studies of the excitation of bound states in the presence of strong perturbations. Unfortunately, the complexity of the corresponding expressions for the projection of the Sturmian basis onto the continuum hydrogenic states has thus far prevented them from performing detailed studies of the ionization.

In this section we show that by representing the Sturmians in momentum space, we can derive exact integral expressions and simple analytical formulas for the projections onto both the bound and continuum states of the hydrogenic basis. These simple expressions relating the Sturmian and hydrogenic basis functions appear to be new and they provide a direct means of comparing the results of the Sturmian calculations with those using the boxed continuum. In addition, they should also prove useful in providing a more detailed interpretation of previous calculations using Sturmian basis functions.

For completeness, we begin this section with a review of the properties of the Sturmian functions in momentum space before deriving explicit expressions for the projections onto the continuum and bound states of the hydrogenic basis.

A. Sturmian functions in momentum space

The Coulomb Sturmians are defined by the eigenvalue equation[23]

$$-\frac{1}{2}\frac{d^2S}{dx^2}-\frac{\alpha}{x}S=\epsilon_0 S, \quad x\geq 0 \tag{41}$$

with $S(x)=0$ for $x\leq 0$. ϵ_0 is a fixed parameter that characterizes a particular basis $\{S_\alpha^{\epsilon_0}(x)\}$ and α are the eigenvalues of the equation that characterize each element of the basis. In other words the Sturmians satisfy a Sturm-Liouville problem where the eigenvalues are the coefficients of the Coulomb potential.

We can easily see that by multiplying Eq. (41) by $1/\alpha^2$ and rescaling x by α we reduce Eq. (41) to the Schrödinger equation, Eq. (6), with $\epsilon=\epsilon_0/\alpha^2$. Therefore the Sturmians are related to the hydrogenic eigenfunctions ϕ_ϵ,

$$S_\alpha^{\epsilon_0}(x)=C\phi_\epsilon(\alpha x)\ , \tag{42}$$

where C is a proportionality constant to be determined by the normalization condition.

Since the parameter ϵ_0 is usually chosen to be negative, the eigenvalues α are completely determined by the negative spectrum of the hydrogen problem, $\epsilon=-1/2n^2$, so defining

$$\alpha_n=\left[\frac{\epsilon_0}{\epsilon}\right]^{1/2}=(2\,|\,\epsilon_0\,|\,)^{1/2}n\ , \tag{43}$$

we have a discrete set of basis functions

$$S_n^{\epsilon_0}(x)=C\phi_n(\alpha_n x)\ . \tag{44}$$

The Sturmian associated with the eigenvalue α_n is obtained directly from making a change of scale of α_n in the argument of the hydrogen eigenfunction ϕ_n. However, the change of scale is different for different n's. This procedure creates a complete basis set out of the discrete hydrogen eigenfunctions only.[23]

For physical interpretation, one usually chooses $\epsilon_0=-1/2n_0^2$ for some initial choice of n_0. Then $\alpha_n=n/n_0$ and $S_{n_0}^{n_0}$ is identical to the eigenfunction that coincides with the hydrogen eigenfunction of the same quantum number n_0, up to a constant arising from the difference in normalization.

To determine the normalization constant C we multiply Eq. (41) for α_n and S_n by S_m^* and subtract from it Eq. (41) for α_m and S_m^*, multiplied by S_n and integrated over x, to obtain

$$(\alpha_m-\alpha_n)\int_0^\infty \frac{S_m^* S_n}{x}dx=\int_0^\infty \left[S_m^*\frac{d^2S_n}{dx^2}-S_n\frac{d^2S_m^*}{dx^2}\right]dx\ . \tag{45}$$

Therefore, since the right-hand side of this equation vanishes upon integration by parts, the $S_n^{n_0}$ can be orthonormalized with the weight $1/x$ (the absolute value of the potential),

$$\left\langle S_n^{n_0}\left|\frac{1}{x}\right|S_m^{n_0}\right\rangle=\delta_{nm}\ . \tag{46}$$

As in the case of the hydrogenic eigenfunctions, it proves more convenient to work in momentum space for the Sturmian description of the one-dimensional hydrogen atom. For that, we will need the momentum-space Sturmians

$$S_n^{n_0}(p)=(2\pi)^{-1/2}\int_0^\infty S_n^{n_0}(x)e^{-ipx}dx\ . \tag{47}$$

From Eq. (44) and Eq. (47) we see that the momentum-space Sturmian is related to the hydrogenic wave function in momentum space by

$$S_n^{n_0}(p)=\frac{C}{\alpha_n}\psi_n\left[\frac{n_0}{n}p\right]\ . \tag{48}$$

So we can use Eq. (11) for the p-space hydrogen wave function $\psi_n(p)$ in Eq. (48) to obtain $S_n^{n_0}(p)$ up to a normalization constant C, which is then obtained by evaluating Eq. (46) in momentum space, using the relation between $1/x$ to p^2 for the Sturmians, given by Eq. (41). Finally, with the resulting value of C, we have

$$S_n^{n_0}(p)=\left[\frac{2n}{\pi}\right]^{1/2}\frac{n_0}{(1+n_0^2p^2)}\exp[2in\cot^{-1}(n_0p)]\ . \tag{49}$$

B. Schrödinger equation in the Sturmian representation

If we expand the wave function $\phi(x,t)$ in the Sturmian basis,

$$\phi(x,t)=\sum_n a_n(t)S_n^{n_0}(x)\ , \tag{50}$$

and substitute it in the Schrödinger equation for our problem, Eq. (2); we get, after making the phase transformation $a_n(t)=e^{it/2n_0^2}b_n(t)$ to simplify the resulting equations,

$$i\sum_n \frac{db_n}{dt}d_{mn}=\sum_n\left[\left[\frac{n}{n_0}-1\right]\delta_{nm}-F(t)\cos(\Omega t)x_{mn}\right]b_n\ , \tag{51}$$

where $d_{mn}=\langle S_m^{n_0}\mid S_n^{n_0}\rangle$ and $x_{mn}=\langle S_m^{n_0}\mid x\mid S_n^{n_0}\rangle$.

C. Matrix elements d_{mn} and x_{mn}

To solve Eq. (51) we need the overlap coefficients between Sturmians d_{mn} and the dipole matrix elements x_{mn}. Using Eq. (49), we can evaluate them by direct integration in momentum space. They can also be calculated directly from the x-space Sturmians.[23] The only nonzero matrix elements are

$$d_{nm}=d_{mn}=\begin{cases} n_0 n & \text{for } m=n \\ -(1/2)n_0[n(n-1)]^{1/2} & \text{for } m=n-1 \\ 0 & \text{otherwise}\ , \end{cases} \tag{52}$$

$$x_{nm}=x_{mn}=\begin{cases} (3/2)n_0^2n^2 & \text{for } m=n \\ -(1/2)n_0^2(2n-1)[n(n-1)]^{1/2} & \\ & \text{for } m=n-1 \\ (1/4)n_0^2(n-1)[n(n-2)]^{1/2} & \text{for } m=n-2 \\ 0 & \text{otherwise}\ . \end{cases} \tag{53}$$

D. Projection of Sturmians onto the hydrogen continuum states

To study the ionization problem in the Sturmian representation, we will need to compute the probability of $\phi(x,t)$ of being in the continuum. To compute this probability, we will need the projection of the Sturmians onto the continuum eigenstates. In this section we will determine the projection matrix elements $\langle S_n^{n_0}\mid\psi_k\rangle$ of the Sturmians onto the continuum.

For calculating the projections, we take Eq. (6) with $\epsilon=k^2/2$ and Eq. (41) with $\alpha=n/n_0$ and $\epsilon_0=-1/2n_0^2$, which are written in operator form as

$$\begin{aligned}&\left[\frac{p^2}{2}-x^{-1}-\frac{k^2}{2}\right]\left|\psi_k\right\rangle=0\ ,\\ &\left[\frac{p^2}{2}-\frac{n}{n_0}x^{-1}+\frac{1}{2n_0^2}\right]\left|S_n^{n_0}\right\rangle=0\ .\end{aligned} \tag{54}$$

Next, we multiply the first equation by n/n_0 and $\langle S_n^{n_0}\mid$ and take the complex conjugate. Then subtracting the second equation multiplied by $\langle\psi_k\mid$ and solving for

$\langle S_n^{n_0} \mid \psi_k \rangle$, we obtain

$$\langle S_n^{n_0} \mid \psi_k \rangle = \frac{n_0(n-n_0)}{(1+nn_0k^2)} \langle S_n^{n_0} \mid p^2 \mid \psi_k \rangle \ . \tag{55}$$

We can see immediately from this last expression that $\langle S_n^{n_0} \mid \psi_k \rangle = 0$ for $n = n_0$. As discussed before, $\mid S_{n_0}^{n_0} \rangle$ is the hydrogen eigenfunction $\mid \psi_{n_0} \rangle$ up to a constant; therefore it is orthogonal to all hydrogen continuum states.

By looking at Eq. (14) for ψ_k, we see that we will make the right-hand-side integral easier to evaluate if we add and subtract k^2 from p^2. The result is

$$\langle S_n^{n_0} \mid \psi_k \rangle = \frac{(n-n_0)n_0}{(1+n_0^2k^2)} \langle S_n^{n_0} \mid p^2-k^2 \mid \psi_k \rangle$$

$$= \frac{2}{\pi} \frac{(n-n_0)n_0^2(nk)^{1/2}}{(1-e^{-2\pi/k})^{1/2}(1+n_0^2k^2)} \int_{-\infty}^{\infty} \frac{\exp\left[i\frac{1}{k}\log\left|\frac{p+k}{p-k}\right| - i2n\cot^{-1}(n_0p)\right]}{(1+n^2p^2)} \exp\left[-\frac{1}{k}\arg\left[\frac{p+k}{p-k}\right]\right] dp \ . \tag{56}$$

For large n and small k, our case of interest, we can apply the method of stationary phase[24] to obtain a very good approximation to this integral. The final result is

$$\langle S_n^{n_0} \mid \psi_k \rangle \simeq 2^{3/2} \left[\frac{k}{\pi}\right]^{1/2} \times \frac{n_0^{5/4}(n-n_0)^{3/4}}{(1+n_0nk^2)^{1/4}(1+n_0^2k^2)(1-e^{-2\pi/k})^{1/2}} \times \cos(\beta+\pi/4) \ , \tag{57}$$

where

$$\beta = -2n\cot^{-1}\{[n_0(1+nn_0k^2)/(n-n_0)]^{1/2}\} + \frac{2}{k}\tanh^{-1}\{k[n_0(n-n_0)/(1+nn_0k^2)]^{1/2}\} \ .$$

In Fig. 4 we show a comparison of Eq. (57) with the results of a direct numerical integration of Eq. (56) which shows that Eq. (57) provides a very good approximation of the projections even for $n = 1$.

E. Projection of Sturmians onto hydrogenic bound states

In this section we will calculate the projection of Sturmians onto the discrete hydrogen states $\langle S_n^{n_0} \mid \psi_m \rangle$. By doing the same analysis with Eq. (6) and Eq. (41), as done in Sec. V D, but now for the negative discrete values of the energy, $\epsilon_m = -1/2m^2$, we obtain the following relation between $\langle S_n^{n_0} \mid \psi_m \rangle$ and $\langle S_n^{n_0} \mid p^2 \mid \psi_m \rangle$:

$$\langle S_n^{n_0} \mid \psi_m \rangle = \frac{n_0m^2(n-n_0)}{(m^2-nn_0)} \langle S_n^{n_0} \mid p^2 \mid \psi_m \rangle \ . \tag{58}$$

Again, the expression above is zero for $n = n_0$ because $\mid S_{n_0}^{n_0} \rangle \propto \mid \psi_{n_0} \rangle$ and it is orthogonal to all other bound states. By looking at Eq. (11) for the discrete eigenfunction ψ_m in momentum representation, we will make the integral easier to evaluate if we relate $\langle S_n^{n_0} \mid \psi_m \rangle$ to $\langle S_n^{n_0} \mid (1+m^2p^2) \mid \psi_m \rangle$. From Eq. (58) we then obtain

$$\langle S_n^{n_0} \mid \psi_m \rangle = \frac{(n-n_0)n_0}{(m^2-n_0^2)} \langle S_n^{n_0} \mid (1+m^2p^2) \mid \psi_m \rangle$$

$$= \frac{2}{\pi}(nm)^{1/2} \frac{(n-n_0)n_0^2}{(m^2-n_0^2)} \int_{-\infty}^{\infty} \frac{\exp[2im\cot^{-1}(mp) - 2in\cot^{-1}(n_0p)]}{(1+n_0^2p^2)} dp \ . \tag{59}$$

Once again, in the case in which $n > n_0$, we can obtain a good analytical approximation to Eq. (59). For large n and m, we can apply the method of stationary phase[24] to obtain the very good approximation to Eq. (59),

$$\langle S_n^{n_0} \mid \psi_m \rangle \simeq \frac{2^{3/2}}{\pi^{1/2}} \frac{n_0^{5/4}m}{(m^2-nn_0)^{1/4}} \times \frac{(n-n_0)^{3/4}}{(m^2-n_0^2)} \cos(\gamma+\pi/4) \ , \tag{60}$$

where

$$\gamma = 2m\cot^{-1}\{[(m^2-nn_0)/n_0(n-n_0)]^{1/2}\} - 2n\cot^{-1}\{[n_0(m^2-nn_0)/m^2(n-n_0)]^{1/2}\} \ . \tag{61}$$

Figure 5 shows a comparison of Eq. (60) with the results of a direct numerical integration of Eq. (59). We can see from this figure that Eq. (60) also provides a very good approximation of the projections even for $n = 1$.

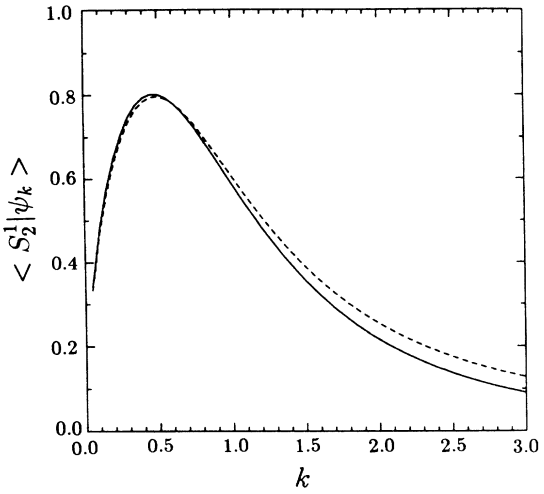

FIG. 4. Approximate formula for the projection matrix elements of Sturmians onto the hydrogenic continuum states, $\langle S_2^1 \mid \psi_k \rangle$, given by Eq. (57) (dashed line) is compared with the numerical integration of the exact expression, given by Eq. (56) (solid line).

F. Numerical algorithm

To study the ionization problem in the Sturmian representation, we choose a reference state n_0, usually the initial state. Then we truncate the Sturmian basis, considering only N_s Sturmians, $S_n^{n_0}$, and we set up the system of ordinary differential equations, Eq. (51), using the overlapping and dipole matrix elements given by Eqs. (52) and (53). We solve for $b_n(t)$ and obtain the ionization probability as

$$P_{\text{ion}} = \int dk \mid \langle \phi \mid \psi_k \rangle \mid^2 , \tag{62}$$

where

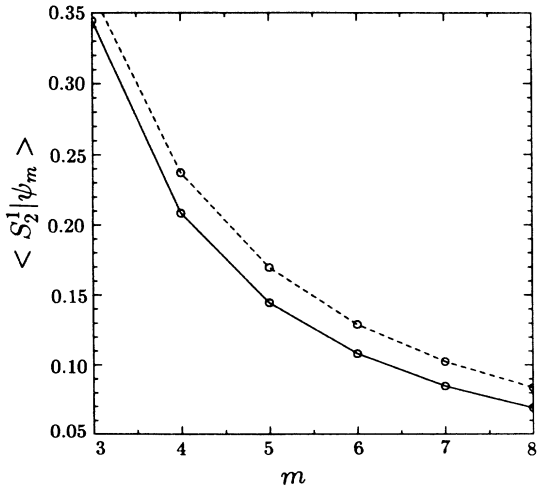

FIG. 5. Approximate formula for the projection matrix elements of Sturmians onto the hydrogenic bound states, $\langle S_2^1 \mid \psi_m \rangle$, given by Eq. (60) (dashed line) is compared with the numerical integration of the exact expression, given by Eq. (59) (solid line).

$$\mid \langle \phi \mid \psi_k \rangle \mid = \left| \sum_n b_n(t) \langle S_n^{n_0} \mid \psi_k \rangle \right| , \tag{63}$$

with the $\langle S_n^{n_0} \mid \psi_k \rangle$ calculated by Eqs. (56) or (57).

VI. RESULTS

To provide a comparison of our three different approaches to the numerical solution of the time-dependent Schrödinger equation for a one-dimensional hydrogen atom in a strong, oscillating electric field, we will examine the results of some typical calculations. For the purposes of illustration we will restrict the discussion here to a specific model problem. This case study will examine the excitation and ionization of a one-dimensional hydrogen atom, initially prepared in the $n_0 = 20$ state, in oscillating fields with a scaled frequency of $n_0^3 \Omega = 1.0$ and with peak amplitudes greater than 10% of the Coulomb binding field.

Although this model problem does not correspond directly to the parameter ranges of the current experiments with either highly excited hydrogen atoms in strong microwave fields or with ground-state atoms in intense laser fields, it provides a single example which exhibits many of the important features of both of these two very different experimental regimes. For example, the ionization of an $n_0 = 20$ hydrogen atom in an oscillating field with a scaled frequency of $n_0^3 \Omega = 1.0$ requires the absorption of a minimum of ten photons. By comparison the laser ionization of ground-state atoms, which has stimulated tremendous excitement in the atomic physics community, typically requires a minimum of 12 photons (for 1096-nm light) for ionization.[25] Therefore, we should expect that our numerical calculations, which include a detailed representation of the coupling to the continuum, will exhibit the multiple above-threshold ionization (ATI) peaks which are characteristic of these experiments.[25] However, because of the anharmonic spacing of the low-lying energy levels only a few bound states are involved in this laser ionization process. In contrast for the $n_0 = 20$ atom this scaled frequency corresponds very closely to the resonant frequencies for single photon transitions to the $n = 19$ and 21 states. As a consequence our numerical calculations for this model problem should also expose the role of the coupling of a large number of bound states in the excitation and ionization of highly excited hydrogen atoms. In these latter experiments hundreds of photons must be absorbed to ionize and 1 to 20 photons are required to excite adjacent bound states. Since the primary purpose of this paper is to lay the foundations for the numerical solution of the time-dependent Schrödinger equation for simple atoms in strong oscillating fields, we will defer the detailed studies of these specific applications to other works.[11,21,26,27]

The algorithms described in Secs. IV and V for the solution of the time-dependent Schrödinger equation, using hydrogenic basis functions with both the $x \cdot E$ and $p \cdot A$ representations of the perturbation and using Sturmian basis functions, were implemented in Fortran codes which were optimized to run on a Cray X-MP/48 using standard library subroutines to solve systems of ordinary

differential equations. These codes were first tested in simple cases, for which analytical results are known. For example all three codes agreed with the predictions of Fermi's golden rule for single photon ionization.

It is interesting to note that already in these simple tests the differences in the effectiveness of the numerical algorithms were readily apparent. In particular, the Sturmian calculations required a basis of 100 Sturmians to recover the Fermi golden rule for single photon ionization of the ground state for ten periods of the perturbation. In contrast the same accuracy could be achieved using the hydrogenic basis with a much smaller basis consisting of a single bound state and ten, carefully chosen, discrete states of the boxed continuum. As a consequence, the straightforward numerical integration of the corresponding systems of ordinary differential equations was found to be much more efficient using the hydrogenic basis functions than with the Sturmians.

A. Calculations using the hydrogenic basis with $x \cdot E$ coupling

As indicated in Sec. I, one of the most striking features of the experiments on the microwave ionization of highly excited hydrogen atoms is the sharp field threshold for the onset of significant ionization which corresponds very closely to the onset of chaotic ionization in the classical theory. One of the primary purposes of our numerical studies of the solution of the corresponding Schrödinger equation is to determine the quantum-mechanical mechanism which is responsible for this sharp ionization threshold which mimics the onset of classical chaos. To this end we have used our codes to perform numerical "experiments" to explore the dependence of the excitation and ionization of one-dimensional hydrogen atoms on the amplitude, frequency, duration, and overall temporal behavior of the oscillating perturbation.

For example, Fig. 6 shows a graph of the natural logarithm of the probability for a one-dimensional hydrogen atom, initially in the $n_0=20$ state, to remain in a bound state, $P_B=\sum_n |a_n|^2$, as a function of time (measured in the number of periods of the oscillating perturbation) for field strengths of $n_0^4F=0.03$, 0.05, and 0.07 (a.u.). (For small levels of ionization this graph can also be interpreted as a plot of the ionization probability as a function of time by taking the absolute value of $\ln P_B$ and an estimate of the ionization rate can be obtained from the slope of a straight-line fit to these curves.)

Several interesting features of physical significance are immediately apparent in these calculations which were performed using a hydrogenic basis of 90 bound states and 100 continuum states in the $x \cdot E$ gauge. First and foremost is the sharp increase in ionization as the field is increased from $n_0^4F=0.05$ to 0.07. After ten periods of a $\cos(\Omega t)$ perturbation which was turned on suddenly at $t=0$, the probability of ionization is only approximately 0.03% for $n_0^4F=0.05$ and is 30 times larger for $n_0^4F=0.07$. It is also noteworthy that, despite the sudden turn-on of the perturbation, approximately five periods elapsed before the ionization began to increase at the larger field. Finally, we note that the fluctuations in the ionization probability indicate that at these high fields the probability oscillates back and forth between the bound and continuum states during each cycle of the perturbing field.

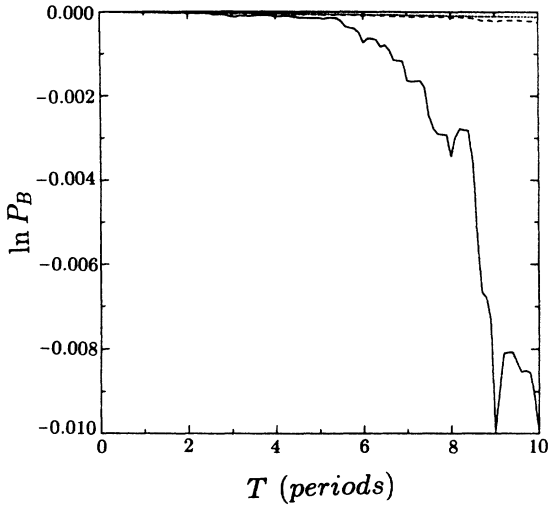

FIG. 6. Natural logarithm of the total probability of remaining bound P_B is plotted vs time for ten periods of a cosine perturbation applied to the $n_0=20$ state with a frequency of $n_0^3\Omega=1.0$ and field strengths of $n_0^4F=0.03$ (dotted line), 0.05 (dashed line), 0.07 (solid line).

In trying to understand the quantum mechanisms which are responsible for these features, our numerical "experiments" have a significant advantage over real experiments since we can perform direct observations of the evolution of the wave function itself. For example, Fig. 7 shows the projections of the wave function after ten periods of the perturbation onto 100 states of the discretized continuum for $n_0^4F=0.03$, 0.05, and 0.07. This

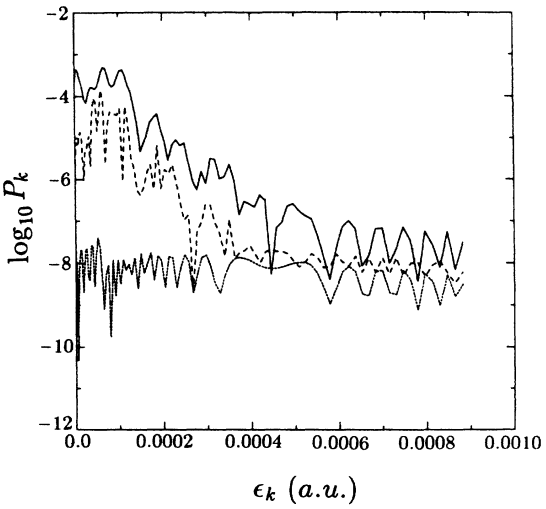

FIG. 7. Log_{10} of the probability of occupying each of the 100 states of the discretized continuum at the end of ten periods of the perturbation for $n_0^4F=0.03$ (dotted line), 0.05 (dashed line), and 0.07 (solid line).

graph plots the normalized amplitude $P_k = |y_k|^2$ of occupying each of the discretized continuum states (defined in Sec. IV B) versus the corresponding energy $\epsilon_k = k^2/2$. In each case the distribution of probability in the continuum exhibits a series of peaks and oscillations which decrease in amplitude with increasing energy into the continuum. The greater ionization at $n_0^4F = 0.07$ is clearly manifest in the order of magnitude increase in the projections onto the continuum states over that for $n_0^4F = 0.05$.

As described in previous work,[11,21] the structure in the continuum for $n_0^4F = 0.07$ can be largely ascribed to a family of peaks associated with multiphoton excitation from highly excited bound states which are replicated at intervals of the photon energy $\epsilon_\Omega = 0.000\,125$ (a.u.). This detailed structure in the continuum energy spectrum shows many of the same features as the experimental ATI spectra.[25] In addition, the observant reader will note that most of the peaks in the continuum do not correspond to an integer number of photons from the initial state but rather to an integer number of photons from a sequence of excited bound states which are also separated in energy by approximately one photon. (See Fig. 8.) Although this result would appear to violate the conservation of energy, the sudden turn-on of the perturbation provides a broad spectrum of photon frequencies which can make up the difference. A slow or adiabatic turn-on and turn-off of the perturbation should modify the structure in the continuum and extensive calculations are currently underway to examine the effect of the temporal evolution of the envelope of the oscillating electric field.[27]

To check for numerical convergence and in particular to check whether the number of discretized continuum states were sufficient to resolve the wave function in the continuum, we increased the density of boxed continuum states in the same energy range to see if both the magnitude and detailed structure of the distribution remained the same. The range of continuum energies was also increased, although in this case it is clear that the higher energies give a negligibly small contribution to the continuum dynamics. Both checks showed that 100 continuum states in an energy range from zero to four times the energy of the state at which the bound-continuum matrix element of the $n_0 = 20$ state achieves its maximum, were sufficient to resolve the detailed structure of the continuum dynamics for 10 to 20 periods of the perturbation. However, for longer calculations the peaks in Fig. 7, which correspond to multiphoton resonances from excited states $n > 20$, grow sharper and a higher density of discretized continuum states are required to resolve them.

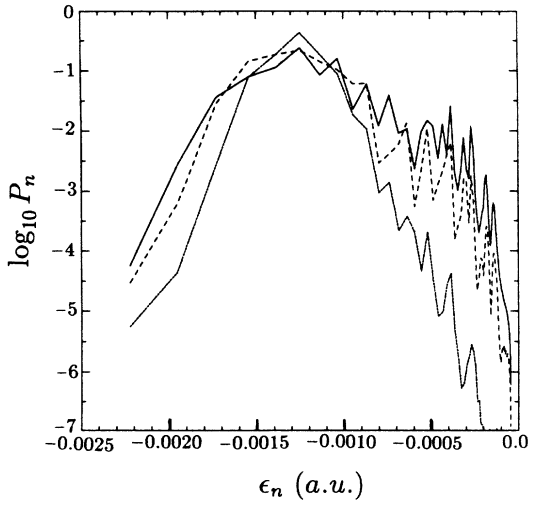

FIG. 8. Log_{10} of the average probability of occupying each of the 90 bound states, $n = 16$–105, at the end of ten periods of the perturbation for $n_0^4F = 0.03$ (dotted line), 0.05 (dashed line), and 0.07 (solid line).

The source of the sharp increase in the ionization at the highest field is readily apparent in Fig. 8 which shows the logarithm of the probability of occupying each of the bound states $P_n = |a_n|^2$ versus energy $\epsilon_n = -1/(2n^2)$ for each of the three field strengths. Since the probabilities of occupying the different bound states exhibit "Rabi-flopping" fluctuations in time, this graph plots a time average of the populations over several periods of the perturbation. For $n_0^4F = 0.03$ the wave function remains highly "localized" to the vicinity of the initial state with an average of approximately 10% probability of occupying the $n = 19$ and 21 states but with probabilities of occupying states with $n < 18$ or $n > 25$ which drop well below 1%. For the higher field of $n_0^4F = 0.05$ the average probability of exciting states with $n > 30$ rises by several orders of magnitude. Finally, for $n_0^4F = 0.07$ the average probability of populating highly excited states rises by another factor of 10, giving population levels of approximately 1% in states as high as $n = 45$.

The sharp increase in the ionization as the field is increased from $n_0^4F = 0.03$ to 0.07 is a direct result of the increased excitation of highly excited states. In particular, a careful examination of the evolution of these excitation curves as a function of time for the highest field reveals that the five period delay in the onset of rapid ionization occurs because several periods of the perturbation must elapse before the probability builds up in these highly excited states. After this build-up time the average probability distribution in highly excited states remains relatively constant except for the slow decay into the continuum.

From these calculations, we conclude that the threshold field for the onset of significant excitation of highly excited states and the associated ionization lies between $n_0^4F = 0.05$ and 0.07. Although this is a factor of 2 larger than the threshold field for the onset of chaotic ionization for $n^3\Omega = 1.0$ and the experimentally measured[6] threshold for $n_0 = 88$ (with $n_0^3\Omega = 1.028$), this discrepancy may be attributed to the low quantum number $n_0 = 20$. Our preliminary investigations[27,28] of the excitation of highly excited states for the experimental parameters[6] using this algorithm, as well as the studies of others,[8–10] all indicate that the one-dimensional quantum calculations for the threshold field for significant excitation corresponds very closely to the experimental measurements and the classical predictions.

B. Calculations using $p \cdot A$ coupling and with the Sturmian basis functions

The same model calculations were also performed using the hydrogenic basis with the $p \cdot A$ coupling to the continuum and with the Sturmian basis functions. Despite the significant differences in the matrix elements and the numerical algorithms all three calculations gave similar results for the excitation and ionization of the $n_0 = 20$ state of the one-dimensional hydrogen atom. In particular, Fig. 9 shows a comparison of all three calculations of the ionization probability (logarithm of the probability of remaining bound) as a function of time for $n_0^4 F = 0.07$.

The $p \cdot A$ calculation was also performed with 90 bound and 100 continuum states; however, the elimination of the diagonal dipole matrix elements permitted the inclusion of the full C-C coupling. The Sturmian calculations also automatically includes the C-C coupling, but because of the inefficiency of the Sturmian calculation a maximum of 100 Sturmians had to be used to keep the runtime under 1 Cray hour.[28]

In Fig. 9 all three calculations exhibit the sudden increase in the ionization probability after five periods of the perturbation to 0.5–1.0% ionization after ten periods. The overall agreement between the three calculations with and without C-C coupling and using both the $x \cdot E$ and $p \cdot A$ gauges is quite good. The discrepancies in the detailed time dependence should not be a cause for concern. The Sturmian calculations are not expected to be as accurate as the hydrogenic basis calculations, since a comparable representation of the relevant bound and continuum states would require at least twice as many Sturmian basis functions. Moreover, the ambiguity in the interpretation of probability in the $p \cdot A$ gauge when the perturbation is on precludes a close comparison of the instantaneous probabilities of occupying either the bound or continuum states. In particular, this aspect of the $p \cdot A$ calculations accounts for the larger oscillations in the ionization probability during each period.[22]

The overall agreement between the three calculations is also exhibited in the average probabilities of occupying each of the bound states from $n = 15$ to 105 shown in Fig. 10 for the hydrogenic and Sturmian calculations in the $x \cdot E$ gauge. In particular, both calculations exhibit comparable levels of excitation in the highly excited states which are responsible for the large levels of ionization. The corresponding results for the $p \cdot A$ calculation are also very similar. (In fact, they were not plotted in Fig. 10 to avoid cluttering the graph.) This later comparison provides a remarkable demonstration of the gauge invariance of the quantum calculations since the diagonal matrix elements, which have been shown to provide a dominant mechanism for the excitation of bound states in the $x \cdot E$ gauge, are totally absent in the $p \cdot A$ calculations. As indicated in the extensive literature on this issue the effects of the missing or reduced matrix elements are compensated by higher-order couplings which must be included in perturbation theory but are automatically incorporated in the numerical solutions.

Finally, Fig. 11 shows the projection of the wave function after 10 periods onto the states of the boxed continuum for all three calculations. Again the overall agreement is quite good. As before, the discrepancy between the Sturmian and hydrogenic calculations can be attributed to the relative inaccuracy of the restricted Sturmian basis. More importantly, the close correspondence of the $x \cdot E$ and $p \cdot A$ results indicate that the C-C interactions do not appear to play an important role in the ionization of the $n_0 = 20$ state at these frequencies and fields in agreement with the conjecture of Blümel and Meir.[20] However, the neglect of the C-C coupling is not always justified,

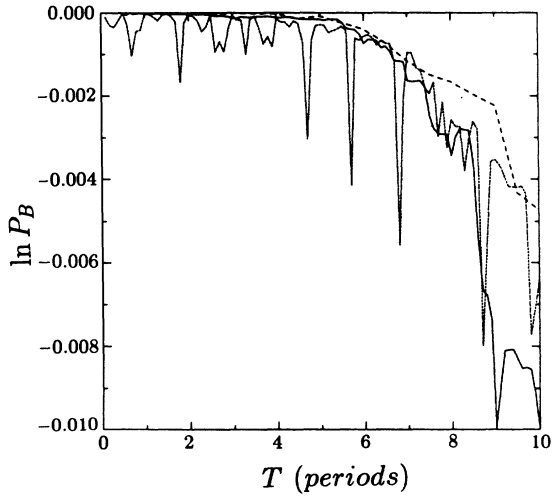

FIG. 9. Natural logarithm of the total probability of remaining bound P_B is plotted vs time for ten periods of the perturbation with $n_0^4 F = 0.07$ using hydrogenic basis states in the $x \cdot E$ gauge (solid line), in the $p \cdot A$ gauge (dotted line), and using 100 Sturmian basis functions in the $x \cdot E$ gauge (dashed line).

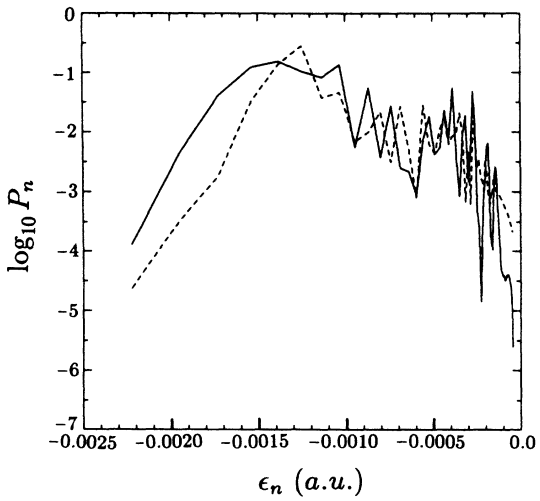

FIG. 10. Log_{10} of the probability of occupying each of the hydrogenic bound states, $n = 16$–105, at the end of ten periods of the perturbation with $n_0^4 F = 0.07$ using the hydrogenic basis (solid line) and using 100 Sturmian basis functions (dashed line).

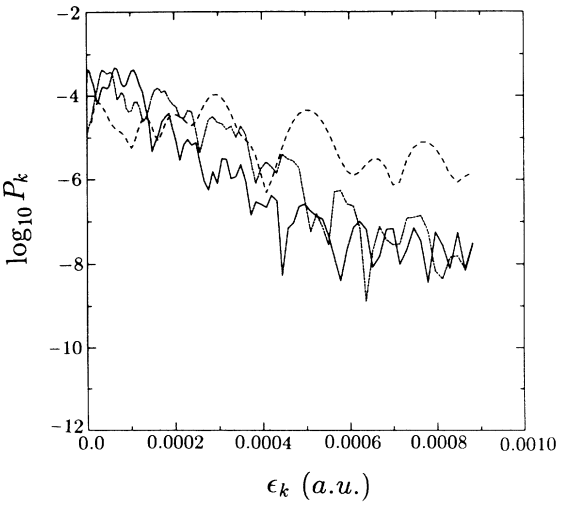

FIG. 11. Log_{10} of the probability of occupying each of the 100 states of the discretized continuum at the end of ten periods of the perturbation with $n_0^4 F = 0.07$ using the hydrogenic basis in the $x \cdot E$ gauge (solid line) and the $p \cdot A$ gauge (dotted line) and using the Sturmian basis functions (dashed line).

since we have shown in Ref. 21 that the inclusion of the C-C interaction can have a profound impact on the details of the excitation of continuum states for the laser ionization of ground-state atoms. In both the Sturmian and $p \cdot A$ calculations the primary role of the C-C interactions for the present parameters is to distribute some of the probability in the continuum to higher energies, which has the effect of reducing the total ionization rate as indicated in Fig. 9.

VII. SUMMARY

Starting from first principles, we have determined exact integral expressions, Eqs. (16), (22), and (26), for the bound-bound, bound-continuum, and continuum-continuum dipole matrix elements for a one-dimensional model of the hydrogen atom. For the large quantum numbers of current interest to the search for "quantum chaos" in the excitation and ionization of highly excited hydrogen atoms, these integral representations are much easier to evaluate and approximate than those expressed in terms of hypergeometric functions. We have also derived simple analytical approximations to the B-B, B-C, and the C-C matrix elements for large n and small k, Eqs. (20), (24), and (28). The derivation of the approximate expressions for the B-B and B-C matrix elements clarifies the range of validity of similar results derived using WKB theory while our expressions for the diagonal and off-diagonal matrix elements for the continuum states are new. These results provide the necessary ingredients for detailed numerical studies of the one-dimensional Schrödinger equation for a one-dimensional hydrogen atom in an oscillating electric field as well as a basis for estimating the relative importance of various quantum processes which affect the onset of chaotic ionization in the experiments with real hydrogen atoms.

We have also described numerical algorithms for studying this problem in both the $x \cdot E$ and $p \cdot A$ gauges which use our results for the various matrix elements along with a natural discretization of the continuum. Since our numerical approach clearly represents the coupling of both the bound states and the continuum states on an equal footing it is easy to assess and control the accuracy of our numerical calculations. For example, we can try to achieve a convergent calculation by independently increasing the numbers of bound and continuum states and we can easily detect the failure of the discretization of the continuum when the density of continuum states is no longer sufficient to resolve the fine structure in the variation of $|b_k|^2$ with k or E_k.

An alternative approach to the calculation of the ionization of atoms in intense fields, which has been pursued by other research groups, is provided by the Sturmian basis functions. Using the momentum-space representation of these basis functions for the one-dimensional hydrogen atom, we have derived convenient new formulas for the projection of the Sturmian states onto the hydrogenic bound and continuum basis states, which enable us to perform the first detailed comparison of these different approaches to the solution of the time-dependent Schrödinger equation.

Together, these programs provide a computer laboratory for investigating the behavior of strongly perturbed quantum systems, which should provide important insight into the microwave ionization problem as well as other physical problems which are not easily treated using perturbation theory. In particular, by directly "observing" the evolution of the quantum-mechanical wave function in both the bound and continuum spaces, we can measure the excitation and ionization, assess the importance of the C-C transitions, examine the different choices of gauge, and study the effects of the temporal behavior of the perturbing field, all as functions of the perturbation frequency and amplitude. Moreover since the method resolves the free electron energy spectrum it can also be used to investigate the quantum mechanisms which underlie the process of above-threshold ionization,[25] which is currently of great interest to researchers studying the interaction of intense laser radiation with atoms. Detailed discussions of the application of our results for the matrix elements and of our numerical algorithms for the solution of the one-dimensional Schrödinger equation is presented in other works.[11,21,26,27]

ACKNOWLEDGMENTS

One of us (S.M.S.) would like to thank Professor Samuel McDowell for useful discussions and suggestions. This research received support from the National Science Foundation. In addition, one of us (R.V.J.) was supported by the Alfred P. Sloan Foundation.

APPENDIX A: NORMALIZATION OF CONTINUUM STATES

To normalize $\psi_k(p)$ in Eq. (12) to a δ function as in Eq. (13), we have to study the asymptotic behavior of $\phi_k(x)$ in the x representation since physically the δ-function

normalization means that far from the origin the wave function behaves as a free wave. Taking Eq. (6) for $\epsilon=k^2/2$ multiplied by $\phi^*_{k'}$ and subtracting its conjugate for $\epsilon'=k'^2/2$ multiplied by ϕ_k, we arrive after integration by parts and rearrangement of terms at[29]

$$\int_0^\xi \phi^*_{k'}(x)\phi_k(x)dx = \frac{1}{(k'^2-k^2)}\left[\phi^*_{k'}\frac{d\phi_k}{dx}-\phi_k\frac{d\phi^*_{k'}}{dx}\right]_{x=\xi} . \quad \text{(A1)}$$

Therefore, we only need the asymptotic expression of ϕ_k for large x to evaluate the integral. For this, it is enough to study the singularities of $\chi_k(\eta)$, the Laplace transform of $\phi_k(x)$.[30] Since we already have $\psi_k(p)$, which is the Fourier transform of ϕ_k, and this latter is different from zero only in the positive half of the x axis, we have the following relation between the Laplace and Fourier transforms of ϕ_k:

$$\chi_k(\eta)=\sqrt{2\pi}\psi_k(-i\eta) = -\sqrt{2\pi}C\frac{1}{(k^2+\eta^2)}\left[\frac{\eta+ik}{\eta-ik}\right]^{i/k} . \quad \text{(A2)}$$

Then we can use Watson's lemma[30] to obtain $\phi_k(x)$ for large x from the expansion of $\chi_k(\eta)$ near its branch points $\eta=\pm ik$:

$$\chi_k(\eta)=\begin{cases} -C\sqrt{2\pi}(\eta+ik)^{i/k-1}(-2ik)^{-i/k-1}+\cdots \\ \qquad\qquad \text{for } \eta\to -ik\ ; \\ -C\sqrt{2\pi}(\eta-ik)^{-i/k-1}(2ik)^{i/k-1}+\cdots \\ \qquad\qquad \text{for } \eta\to ik\ . \end{cases} \quad \text{(A3)}$$

Since the branch points are purely imaginary both expansions contribute equally to the asymptotic form of $\phi_k(x)$. The result after applying Watson's lemma is

$$\phi_k(x)=-C\sqrt{2\pi}\left[\frac{e^{-ikx}(-2ik)^{-i/k-1}}{\Gamma(1-i/k)x^{i/k}}+\cdots + \frac{e^{ikx}(2ik)^{i/k-1}}{\Gamma(1+i/k)x^{i/k}}+\cdots\right] \quad \text{(A4)}$$

which after some rearrangements and simplifications leads to the familiar form of $\phi_k(x)$ for large x derived from the asymptotic form of the confluent hypergeometric function representation of the continuum functions[31]

$$\phi_k(x)=-C\sqrt{2\pi}\frac{e^{-\pi/2k}}{k\,|\,\Gamma(1-i/k)\,|}\times\sin\left[kx+\frac{1}{k}\ln(2kx)+\arg\Gamma(1-i/k)\right] . \quad \text{(A5)}$$

Finally, substituting Eq. (A5) back into Eq. (A1), and taking the limit $\xi\to\infty$, we get after some calculations

$$\int_0^\infty \phi^*_{k'}\phi_k dx = \frac{\pi^2\,|\,C\,|^2 e^{-\pi/2k}e^{-\pi/2k'}}{kk'\,|\,\Gamma(1-i/k)\,|\,|\,\Gamma(1-i/k')\,|}\delta(k'-k) , \quad \text{(A6)}$$

where we have used the fact that

$$\lim_{\xi\to\infty}\sin[(k'-k)f(\xi)]/(k'-k)=\pi\delta(k'-k)$$

when $f(\xi)\to\infty$ as $\xi\to\infty$. Since $|\,\Gamma(1-i/k)\,|^2=\pi/[k\sinh(\pi/k)]$,[32] we only need to equate the coefficient of the δ to 1 to obtain the desired value of C,

$$C=\left[\frac{2k}{\pi}\right]^{1/2}\frac{1}{(1-e^{-2\pi/k})^{1/2}} . \quad \text{(A7)}$$

Substituting this value back into Eq. (A5), we also obtain the well-known asymptotic expression

$$\phi_k(x)=-\left[\frac{2}{\pi}\right]^{1/2}\sin\left[kx+\frac{1}{k}\ln(2kx)+\arg\Gamma(1-i/k)\right] . \quad \text{(A8)}$$

APPENDIX B: CONTINUUM DIAGONAL MATRIX ELEMENTS

The general solution of Eq. (15) for $\langle k'\,|\,x\,|\,k\rangle$ in terms of $\langle k'\,|\,p\,|\,k\rangle$ is

$$\langle k'\,|\,x\,|\,k\rangle=-\frac{2i\langle k'\,|\,p\,|\,k\rangle}{(k'^2-k^2)}+D(k)\delta(k'-k) \quad \text{(B1)}$$

since the δ-function term is identically zero when multiplied by $(k'-k)$. Here we have simply expressed Eq. (15) in terms of the label k corresponding to $\epsilon=k^2/2$.

To compute the actual value of $D(k)$, we will proceed in an analytical way similar to the one used in Appendix A to calculate the normalization in the continuum. We will use the asymptotic form, for large x, of the solution in the continuum $\phi_k(x)$, together with an integration by parts argument, to obtain Eq. (B1). The second term in Eq. (B1) will arise then as the limiting form for large x of the surface term.

We take Eq. (6) for $\epsilon=k^2/2$,

$$-\frac{1}{2}\frac{d^2\phi_k}{dx^2}-\frac{1}{x}\phi_k=\frac{k^2}{2}\phi_k , \quad \text{(B2)}$$

multiply it by $x\phi^*_{k'}$ and subtract the conjugate of Eq. (6) for k' multiplied by $x\phi_k$. After integrating by parts we arrive at

$$\int_0^\xi \phi^*_{k'}x\phi_k dx = -\frac{1}{(k'^2-k^2)}\int_0^\xi\left[\phi^*_{k'}\frac{d\phi_k}{dx}-\phi_k\frac{d\phi^*_{k'}}{dx}\right]dx + \frac{1}{(k'^2-k^2)}\times\left[\phi^*_{k'}x\frac{d\phi_k}{dx}-\phi_k x\frac{d\phi^*_{k'}}{dx}\right]_{x=\xi} . \quad \text{(B3)}$$

Therefore we only need to compute the limit $\xi\to\infty$ of the right-hand side of Eq. (B3) to evaluate $\langle k' \mid x \mid k \rangle$.

However, the only instance in which $\langle k' \mid x \mid k \rangle$ will be used is under an integral over k' (or k), as in the second term of the right-hand side of Eq. (5),

$$\int_{k-\Delta/2}^{k+\Delta/2} e^{i\omega_{kk'}t} b_{k'}(t) x_{kk'} dk' \ . \tag{B4}$$

If we choose Δ such that for all t, $e^{i\omega_{kk'}t} b_{k'}(t)$ varies little in the interval $[k+\Delta/2, k-\Delta/2]$, we are left to calculate

$$\int_{k-\Delta/2}^{k+\Delta/2} x_{kk'} dk' = \int_{k-\Delta/2}^{k+\Delta/2} dk' \int_0^{\xi} dx \ \phi_{k'}^* x \phi_k \ , \tag{B5}$$

with $\Delta \ll k$. To calculate Eq. (B5) we use Eq. (B3) to get

$$\int_{k-\Delta/2}^{k+\Delta/2} x_{kk'} dk' = -\lim_{\xi\to\infty} \int_{k-\Delta/2}^{k+\Delta/2} dk' \frac{1}{(k'^2-k^2)} \int_0^{\xi} dx \left[\phi_{k'}^* \frac{d\phi_k}{dx} - \phi_k \frac{d\phi_{k'}^*}{dx} \right] + \int_{k-\Delta/2}^{k+\Delta/2} dk' \lim_{\xi\to\infty} \frac{1}{(k'^2-k^2)} \left[\phi_{k'}^* x \frac{d\phi_k}{dx} - \phi_k x \frac{d\phi_{k'}^*}{dx} \right]_{x=\xi} . \tag{B6}$$

We then compute the first term by reversing the order of the integrals in k' and x. In this way, we need to compute first

$$\int_{k-\Delta/2}^{k+\Delta/2} dk' \frac{\phi_{k'}^*}{(k'^2-k^2)} \tag{B7}$$

and its derivative with respect to x. For this we use the asymptotic form of $\phi_{k'}^*$ for large x, Eq. (A8). For $\Delta \ll k$ we have, neglecting terms in Δ/k,

$$\int_{k-\Delta/2}^{k+\Delta/2} dk' \frac{\phi_{k'}^*}{(k'^2-k^2)} = -\left[\frac{2}{\pi}\right]^{1/2} \frac{1}{2k} \cos\left[kx + \frac{1}{k}\ln(2kx) + \arg\Gamma(1-i/k) \right] \times \int_{-\Delta/2}^{+\Delta/2} d\eta \frac{\sin(\eta x)}{\eta} \ . \tag{B8}$$

Now, since x is large, the last integral can be approximated by π. So

$$\int_{k-\Delta/2}^{k+\Delta/2} dk' \frac{\phi_{k'}^*}{(k'^2-k^2)} = -\left[\frac{\pi}{2}\right]^{1/2} \frac{1}{k} \cos\left[kx + \frac{1}{k}\ln(2kx) + \arg\Gamma(1-i/k) \right] , \tag{B9}$$

and using this result to evaluate the first term of Eq. (B3) we get

$$-\int_{k-\Delta/2}^{k+\Delta/2} dk' \frac{1}{(k'^2-k^2)} \times \int_0^{\xi} dx \left[\phi_{k'}^* \frac{d\phi_k}{dx} - \phi_k \frac{d\phi_{k'}^*}{dx} \right] = -\xi \ . \tag{B10}$$

In the second term in Eq. (B3), we are multiplying asymptotic expressions by x, which requires asymptotic expressions up to order $1/x$. That is, we need one order of correction more than in Eq. (A8). After computing an extra term in the asymptotic expansion of the Laplace transform $\chi_k(\eta)$ for $\eta\to 0$ and using Watson's lemma again, we have, for $x\to\infty$,

$$\phi_k(x) = -\left[\frac{2}{\pi}\right]^{1/2} \sin\left[kx + \frac{1}{k}\ln x + \alpha_k \right] + \left[\frac{2}{\pi}\right]^{1/2} \frac{1}{2k^2 x} \sin\left[kx + \frac{1}{k}\ln x + \alpha_k \right] - \left[\frac{2}{\pi}\right]^{1/2} \frac{1}{2k^3 x} \cos\left[kx + \frac{1}{k}\ln x + \alpha_k \right] , \tag{B11}$$

where we defined

$$\alpha_k \equiv \frac{1}{k}\ln(2k) + \arg\Gamma(1-i/k) \ .$$

There appear then two extra terms of order $1/x$ to add up to Eq. (A8) to obtain $\phi_k(x)$ to that order. Substituting Eq. (B11) in the integrand of the second term of Eq. (B6), we obtain to lowest order in $1/x$, after having suppressed terms with limit zero in the generalized function sense,

$$\lim_{\xi\to\infty} \frac{1}{(k'^2-k^2)} \left[\phi_{k'}^* x \frac{d\phi_k}{dx} - \phi_k x \frac{d\phi_{k'}^*}{dx} \right]_{x=\xi} = \frac{1}{\pi} \lim_{\xi\to\infty} \frac{\xi}{(k'-k)} \sin\left[(k'-k)\xi + \left[\frac{1}{k'} - \frac{1}{k}\right]\ln\xi + \alpha_k' - \alpha_k \right] = \lim_{\xi\to\infty} \xi\delta(k'-k) \ . \tag{B12}$$

Finally, after integration in k', we get ξ, which cancels out the contribution from Eq. (B10).

*Present address: Princeton Plasma Physics Laboratory, Princeton, NJ 08544.

[1]See, for example, *Chaotic Behavior in Quantum Systems*, edited by G. Casati (Plenum, New York, 1985).

[2]J. E. Bayfield and P. M. Koch, Phys. Rev. Lett. **33**, 258 (1974); J. E. Bayfield, L. D. Gardner, and P. M. Koch, *ibid.* **39**, 76 (1977).

[3]J. G. Leopold and I. C. Percival, J. Phys. B **12**, 709 (1979); J. G. Leopold and D. Richards, *ibid.* **19**, 1125 (1986).

[4]R. V. Jensen, Phys. Rev. Lett. **49**, 1365 (1982); Phys. Rev. A **30**, 386 (1984).

[5]N. B. Delone, V. P. Krainov, and D. L. Shepelyansky, Usp. Fiz. Nauk **140**, 355 (1983) [Sov. Phys.—Usp. **26**, 551 (1983)].

[6]K. A. H. van Leeuwen, G.v. Oppen, S. Renwick, J. B. Bowlin, P. M. Koch, R. V. Jensen, O. Rath, D. Richards, and J. G. Leopold, Phys. Rev. Lett. **55**, 2231 (1985); P. M. Koch *et al.*, in *Physics of Phase Space*, edited by Y. S. Kim and W. W. Zachary (Springer, New York, 1987), p. 106.

[7]J. E. Bayfield and L. A. Pinnaduwage, Phys. Rev. Lett. **54**, 313 (1985); J. N. Bardsley and B. Sundaram, Phys. Rev. A **32**, 689 (1985).

[8]G. Casati, B. V. Chirikov, and D. L. Shepelyansky, Phys. Rev. Lett. **53**, 2525 (1984); G. Casati, B. V. Chirikov, D. L. Shepelyansky, and I. Guarneri, *ibid.* **57**, 823 (1986); Phys. Rep. **154**, 77 (1987).

[9]J. N. Bardsley, B. Sundaram, L. A. Pinnaduwage, and J. E. Bayfield, Phys. Rev. Lett. **56**, 1007 (1986); J. N. Bardsley and M. J. Comella J. Phys. B **19**, L565 (1986).

[10]R. Blümel and U. Smilansky, Phys. Rev. A **32**, 1900 (1985); Z. Phys. D **6**, 83 (1987).

[11]R. V. Jensen, Phys. Scr. **35**, 668 (1987); R. V. Jensen and S. M. Susskind, in *Photons and Continuum States of Atoms and Molecules*, edited by N. K. Rahman, C. Guidotti, and M. Allegrini (Springer, New York, 1987), p. 13.

[12]W. Gordon, Ann. Phys. (Leipzig) **2**, 1031 (1929); see also V. B. Berestetskii *et al.*, *Quantum Electrodynamics*, 2nd ed. (Pergamon, Oxford, 1982), p. 192.

[13]L. D. Landau and E. M. Lifshitz, *Quantum Mechanics*, 3rd ed. (Pergamon, Oxford, 1977).

[14]S. P. Goreslavskii, N. B. Delone, and V. P. Krainov, Zh. Èksp. Teor. Fiz. **82**, 1789 (1982) [Sov. Phys.—JETP **55**, 1032 (1982)].

[15]The momentum-space wave functions for the discrete spectrum of the three-dimensional hydrogen atom were first obtained by B. Podolsky and L. Pauling [Phys. Rev. **34**, 109 (1929)] by a direct transformation of the position-space wave functions. They can also be obtained directly from the Schrödinger equation, which in momentum space reduces to a second-order differential equation by the so-called Hylleraas method: E. Hylleraas, Z. Phys. **74**, 216 (1932); see also M. J. Englefield, *Group Theory and the Coulomb Problem* (Wiley, New York, 1972), Chaps. 4 and 5; and H. A. Bethe and E. E. Salpeter, *Quantum Mechanics of One- and Two-Electron Atoms*, 2nd ed. (Pergamon, Oxford, 1982), Secs. 8 and 9. That the equation reduces to a first order differential equation in one dimension was first shown by E. V. Ivash [Am. J. Phys. **40**, 1095 (1972)].

[16]The discrete spectrum was studied in this way by E. V. Ivash, Ref. 15, which we reproduce here for the sake of completeness.

[17]I. S. Gradshteyn and I. M. Ryzhik, *Table of Integrals, Series and Products* (Academic, New York, 1980), p. 420.

[18]Y. Gontier (private communication).

[19]R. D. Cowan, *The Theory of Atomic Structure* (University of California, Berkeley, 1981), p. 535.

[20]R. Blümel and R. Meir, J. Phys. B **18**, 2525 (1985).

[21]R. V. Jensen and S. M. Susskind, in *Atomic and Molecular Processes with Short Intense Laser Pulses*, edited by A. D. Bandrauk (Plenum, New York, 1988).

[22]J. Javanainen (unpublished).

[23]M. Rotenberg, Adv. At. Mol. Phys. **6**, 233 (1970); A. R. Edmonds, J. Phys. B **6**, 1603 (1973).

[24]N. G. de Bruijn, *Asymptotic Methods in Analysis* (Dover, New York, 1981).

[25]See, for example, Z. Deng and J. H. Eberly, J. Opt. Soc. Am. B **2**, 486 (1985), and references therein; *Atomic and Molecular Processes with Short Intense Laser Pulses*, edited by A. D. Bandrauk (Plenum, New York, 1988).

[26]S. M. Susskind, Ph.D. thesis, Yale University, 1987.

[27]R. V. Jensen and S. M. Susskind (unpublished).

[28]The success of the extensive studies using Sturmian basis functions by Casati *et al.* (Ref. 8) can be attributed to their use of a special numerical algorithm for integrating the associated system of differential equations. We used a standard numerical package for integrating the equations for both the hydrogenic and Sturmian bases, which proved to be prohibitively slow for extensive Sturmian calculations. We hope to pursue both calculations using the algorithm of Ref. 8 in the future.

[29]W. Pauli, in *Pauli Lectures on Physics*, 4th ed., edited by C. P. Enz (MIT, Cambridge, 1981), Vol. 5, p. 185.

[30]B. Davies, *Integral Transforms and Their Applications* (Springer, New York, 1978), p. 84.

[31]L. D. Landau and E. M. Lifshitz, Ref. 13, p. 122.

[32]*Handbook of Mathematical Functions*, edited by M. Abramowitz and I. Stegun (U.S. GPO, Washington, D.C., 1972), p. 256.